MAPPING WATER QUALITY WITH DRONES:

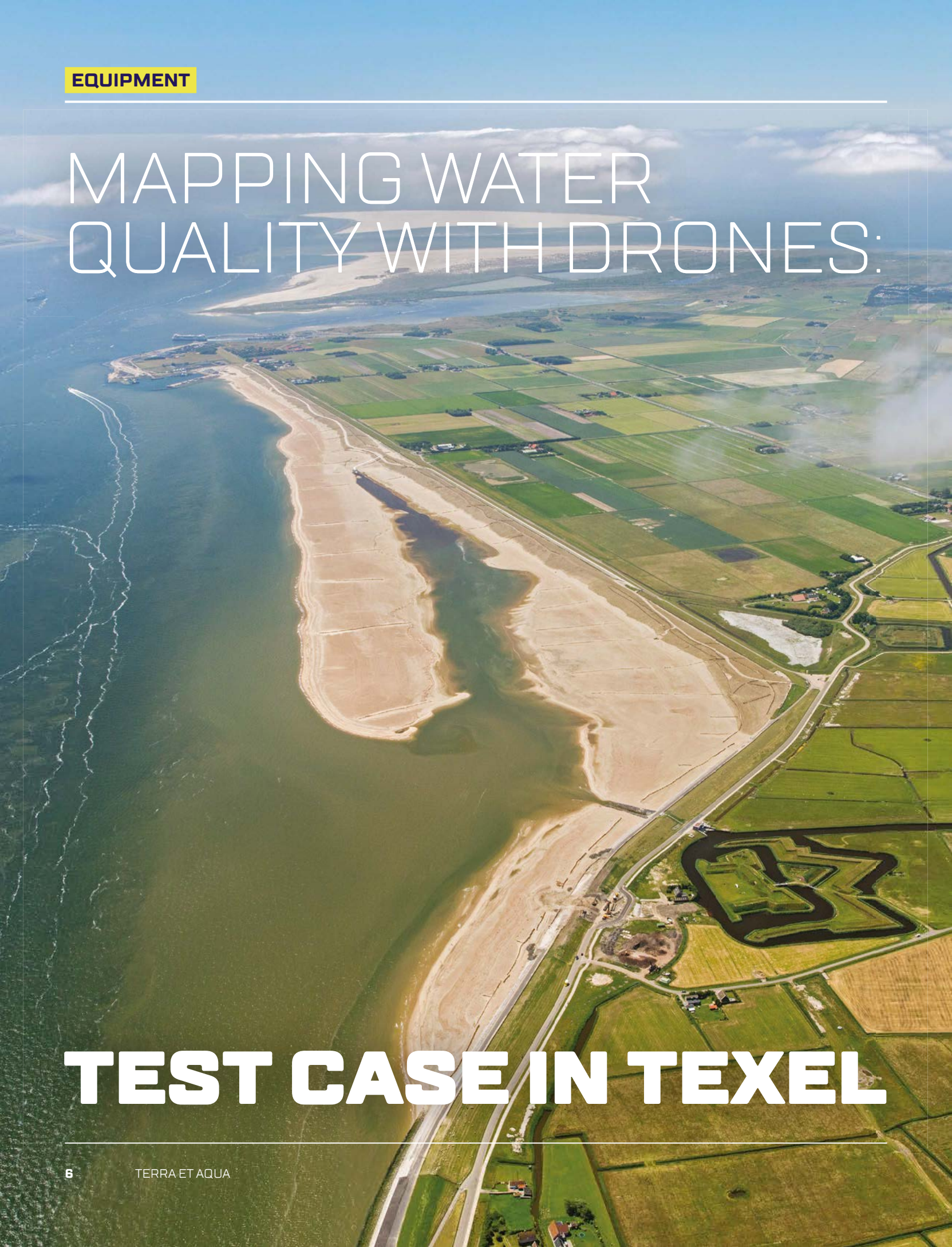

TEST CASE IN TEXEL

To demonstrate drone technology for water quality monitoring, a pilot test case was organised at the Prins Hendrik Zanddijk project in Texel, The Netherlands. Jan De Nul was working on creating a new dune area seaward of the existing dyke. The dune takes over the coastal protection function of the existing dyke and combines it with nature development, public services and recreational appeal.

Waves and white caps, typical for waters with a high dynamic nature, or bottom effects in shallow and clear waters, can alter the signal detected by the sensor.

Challenges in data collection

Recent advances in Remotely Piloted Aircraft Systems (RPAS), or airborne drones, have created an additional monitoring platform that provides an opportunity to capture spatial, spectral and temporal information that could benefit a wide range of applications. This with a relative small investment, especially compared to the cost of manned airborne systems or satellite missions. Drone systems are characterised by a high versatility, adaptability and flexibility and can be rapidly and repeatedly deployed for high spatial and temporal resolution data. They facilitate the collection of information in hard to reach or physically inaccessible areas, and under clouded circumstances.

Drone mapping over water

Although drone mapping over land is becoming more and more common practice (e.g. Ishida et al, 2018; Han et al, 2017), their use for water applications is lagging behind. The additional challenges faced when looking at water surfaces are certainly not an asset in this regard. First of all, water is a dynamic medium subjected to tides, waves, floating and settling particles and many more. The typically used geo-referencing technique, i.e. structure for motion (Westoby *et al*., 2012), which looks at recognisable features within images to stitch these together into a mosaic, is thus not suitable for water. To know which part of the water surface your drone image captures, you fully rely on the Global Positioning System (GPS) with Inertial Measurement Unit (IMU) available on the drone platform. The second challenge is related to the optical properties of water bodies. Water surfaces act as a mirror. When sun light is reflected at the water surface and captured by the sensor, also called sun glint, this results in a gleaming colouring from which it is hard to obtain information on bio-physical properties of the water column itself (Kay et al., 2009). By adapting the flight plan accordingly, tilting the camera slightly and looking away from the sun, this can be avoided as much as possible. But also light scattered in the atmosphere (sky) itself and reflected at the water surface is detected by the sensor and adds a signal that is not related to the water column either. This phenomenon is called sky glint. The processing chain presented in this work corrects for these effects by simulating the cloud conditions and modelling the resulted reflectance signal of the water. This is done using an adapted version of the iCOR tool (De Keukelaere et al., 2017) for airborne drones. Waves and white caps, typical for waters with a high dynamic nature, or bottom effects in shallow and clear waters, can alter the signal detected by the sensor. Through filtering techniques these unwanted effects can be cancelled out. Since water itself is a strongly absorbing feature with low reflectance, the optical sensor has to be able to capture a low signal and noise can become more prominent (low signal to noise ratio).

The technology was tested in Texel, The Netherlands, where dune construction works were taking place. To estimate the impact of the construction activities on the water quality, monitoring efforts were established. Adding drone imagery to this database provides additional information on the spatial gradient of water quality at the surface. By tackling the aforementioned challenges one by one, raw drone data were converted into turbidity maps. At the end, a validation was performed with in-situ data collected simultaneously with the drone flights.

Field campaign

Test site: Texel, The Netherlands

The test was performed in Texel, The Netherlands, where dredging company Jan De Nul Group was working on the Prins Hendrik Zanddijk project. The existing dyke did not meet the requirements for coastal protection any more. In this project a new 3.2-kilometre long dune was being constructed, providing coastal protection combined with nature development, public services and recreational appeal. Soft sand used for construction was gathered at two locations offshore: Den Helder and Terschelling. Fine sediments are discharged with the overflow at the borrow area and coarser sand particles were transported to the reclamation site with the Trailer Suction Hopper Dredger Bartolomeu Dias (see Figure 1). At the dyke's construction site, the heavy sand is pumped ashore through a pipeline while earthmover machinery put all sand in place. Marram grass and sea buckthorn planted on top will reduce sand drift. The Wadden Sea area belongs to the marine world heritage of UNESCO.

The Prins Hendrik Zanddijk project was selected as test case for its convenience (not too far and easy access) but the methodology can be easily adapted to high sensitive areas like the vicinity of coral reefs or aquaculture sites. While current monitoring efforts can be quite intensive if one has to navigate from one buoy to another to collect data, drones can facilitate this process by providing a detailed spatial overview of the sediment plume at the surface.

A set of truecolour Sentinel-2 satellite images shows the progress of the construction works from August to November 2018 (see Figure 2). This satellite sensor contains spectral bands with a spatial

TABLE 1

Nomenclature

AIS	Automatic Identification System
DN	Digital Number
EEdd	Downwelling irradiance
FNU	Formazin Nephelometric Units
FSF	Field Spectroscopy Facility
GPS	Global Positioning System
IMU	Inertial Measurement Unit
LUT	Look-Up-Tables
L_{atm}	Atmospheric radiance
$L_{at-sens}$	At-sensor radiance
$L_{r,sky}$	Sky glint
$L_{r,sun}$	Sun glint
L_{spec}	Radiance from specular reflection at the water surface
L_w	Water-leaving radiance
MODTRAN5	Moderate-Resolution Atmospheric Radiance and Transmittance Model – version 5
NERC	Natural Environment Research Council
NIR	Near-Infrared
NTU	Nephelometric Turbidity Units
RPAS	Remotely Piloted Aircraft Systems
T	Turbidity
TSS	Total Suspended Solids
UTC	Coordinated Universal Time
ρ_w	Water-leaving reflectance
λ	Wavelength

FIGURE 1

Coarser sand particles were transported to the reclamation site with the Trailer Suction Hopper Dredger Bartolomeu Dias (A) and earthmover machinery put all sand in place (B).

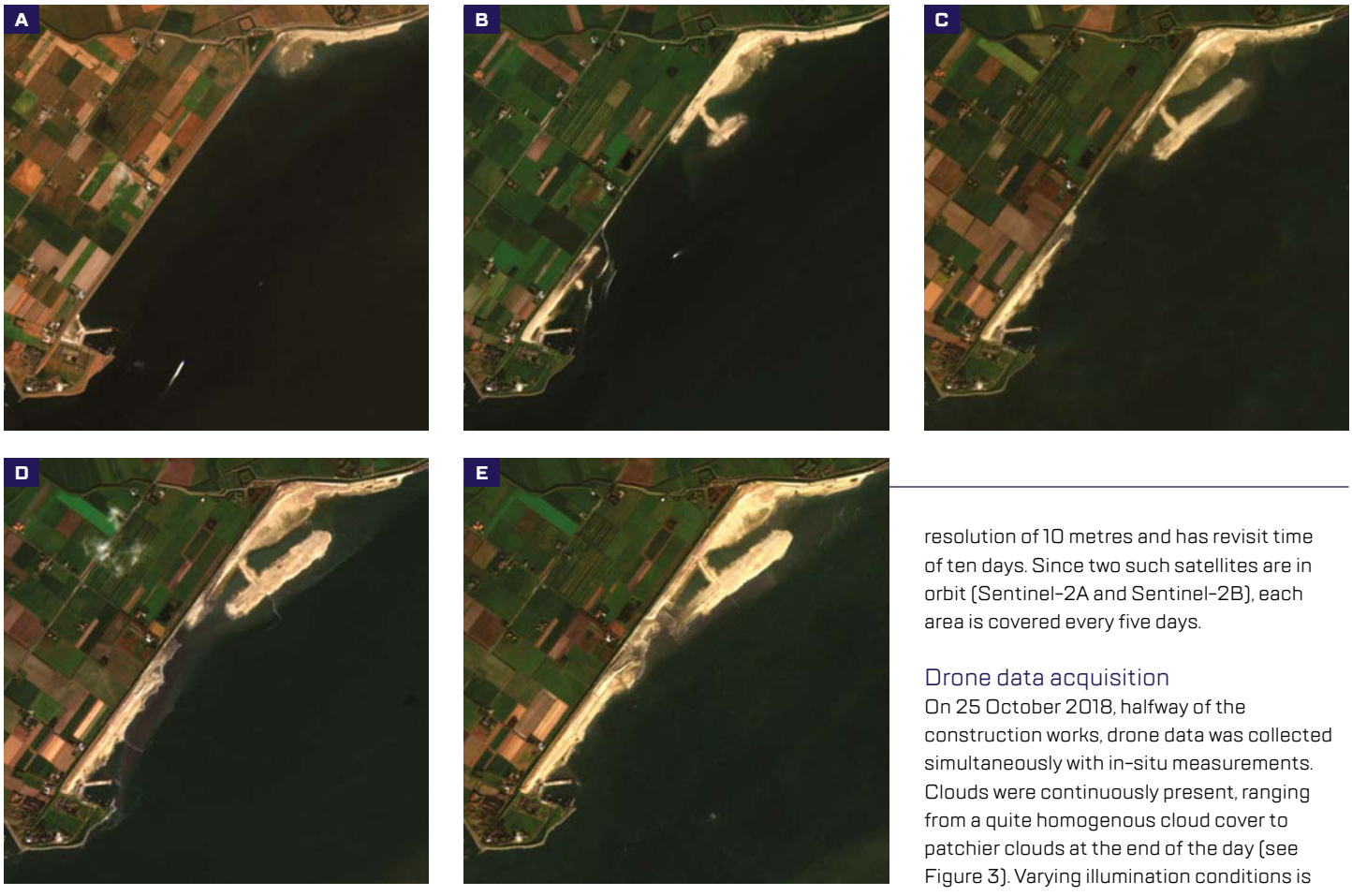

FIGURE 2

Progress of dune construction in Texel (NL) as observed by Sentinel-2. Dates of image acquisition (in 2018: 04/08 (A), 13/09 (B), 13/10 (C), 28/10 (D), 17/11 (E).

resolution of 10 metres and has revisit time of ten days. Since two such satellites are in orbit (Sentinel-2A and Sentinel-2B), each area is covered every five days.

Drone data acquisition

On 25 October 2018, halfway of the construction works, drone data was collected simultaneously with in-situ measurements. Clouds were continuously present, ranging from a quite homogenous cloud cover to patchier clouds at the end of the day (see Figure 3). Varying illumination conditions is an additional challenge when working with optical sensors.

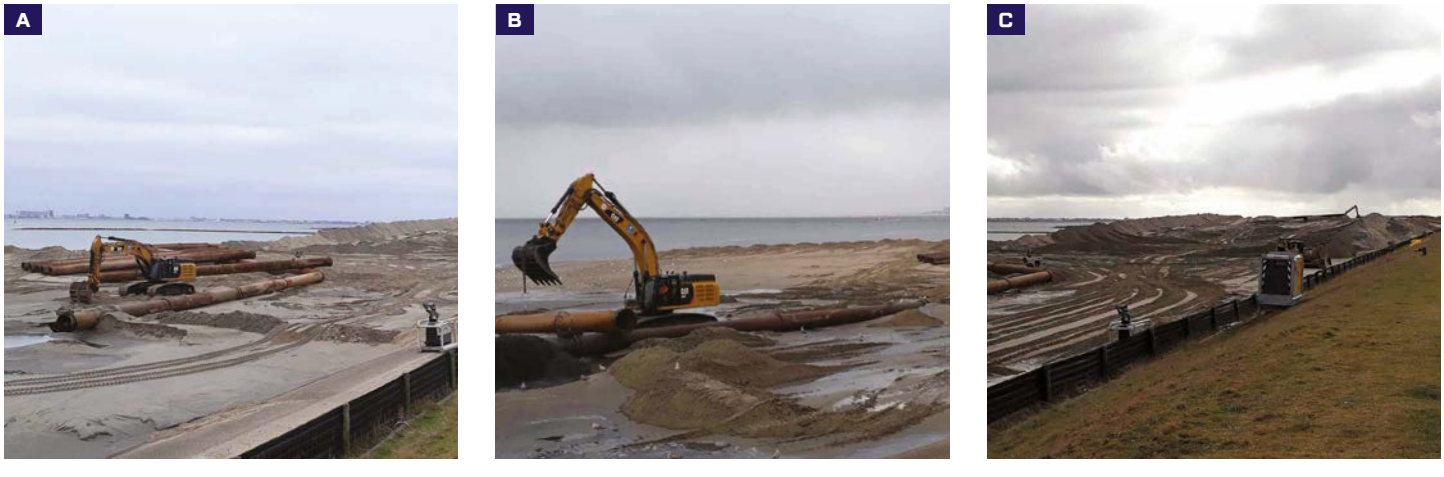

FIGURE 3

Cloud coverage at various moments throughout the day: 7:51 (A), 10:10 (B), 13:27 (C). Hours are expressed in Coordinated Universal Time (UTC).

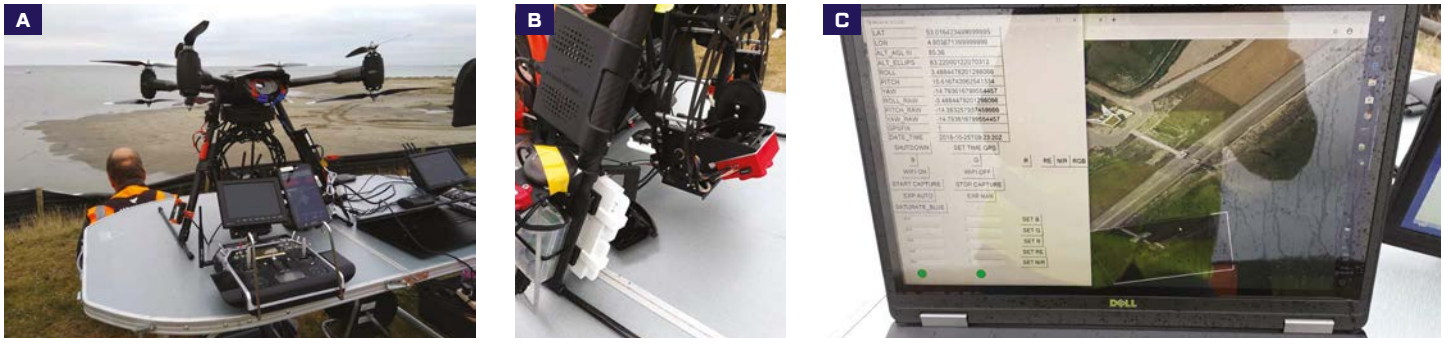

FIGURE 4

Airborne drone platform with controller (A), the payload with multispectral camera, GPS/IMU and irradiance sensor (B), and the base station showing real-time information of the drone flight (C).

An octocopter platform (Altura Zenith ATX-8) with a multispectral camera (MicaSense RedEdge-M) onboard performed the different test flights. The advantages of a multispectral camera are the availability of small spectral bands and the additional bands in the Near-Infrared (NIR) and Red-Edge region. The small bands make it easier to detect specific features, while the addition of the NIR and Red-Edge makes the camera suitable for water quality monitoring in low as well as high turbid regions. Compared to a default RGB camera, this multispectral sensor adds the possibility to derive additional parameters such as the chlorophyll-a concentration. The camera has been calibrated in the Natural Environment Research Council (NERC) Field Spectroscopy Facility (FSF) lab in Scotland to understand its sensitivity over the optical range. During flight operations the camera is slightly tilted and looks away from the sun. This is to avoid the reflection of direct sun light into the field of view of the sensor, a phenomenon called sun glint. Besides the camera, an additional GPS with IMU is attached to allow a better geometric correction. The GPS/IMU collects information on the latitude, longitude and flying height of drone, as well as the roll, pitch and yaw of the camera. Finally, an irradiance sensor is included to obtain information on changing light conditions.

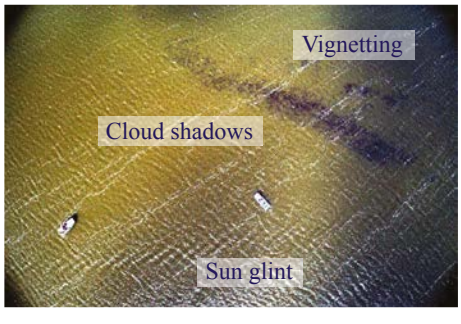

FIGURE 5

Example of an uncorrected truecolour image captured with the MicaSense RedEdge camera. The image shows vignetting effects towards the edges, sun glint effect at the bottom and cloud shadows in the middle of the picture.

Figure 4 shows the system set-up, including the used drone platform with pilot controller and the payload mounted underneath. The right image shows the base stations, which contains real-time information of the drone location, a projected truecolour image, the camera settings and position of neighbouring boats through Automatic Identification System (AIS). With this information, flight missions can be easily adapted and camera settings changed during flights. This allows a large flexibility in flight operations, leaving space to respond rapidly on events or interesting features.

Reference in-situ data

Simultaneously with drone data acquisition, in-situ data were collected for validation of the drone derived data. Turbidity data was obtained every five seconds using a multiparameter sensor, units expressed in Nephelometric Turbidity Units (NTU), according to the EPA 180.1 method (EPA, 1993). Samples from the water surface and dredged material were taken and analysed into resp. Total Suspended Solid (TSS) concentrations and particles size distribution. The particle size distribution of the transported sand yielded d50 values (i.e. the median diameter of the sample's mass) between 298 µm and 414 µm.

Data processing

The collected airborne drone imagery contains raw information expressed in Digital Numbers (DN) and is subjected to distortions from the camera as well as the atmosphere in between the target and the sensor. Figure 5 shows an example from a Scottish lake of an enhanced uncorrected truecolour image, which suffers from vignetting effects (i.e. darkening towards the edges of the image), sun glint effects at the bottom of the image and cloud shadow in the middle of the image. When not properly corrected for, inadequate results will be obtained.

Figure 6 shows the schematic overview of the drone image processing chain to convert raw airborne drone data into meaningful bio-physical data. The chain consists of three main steps, radiometric correction, geo-referencing and turbidity/algorithm (Raymaekers et al., 2017). The different steps are discussed in more detail in the next paragraphs.

Radiometric correction

The radiometric step converts the raw drone imagery from digital numbers to water

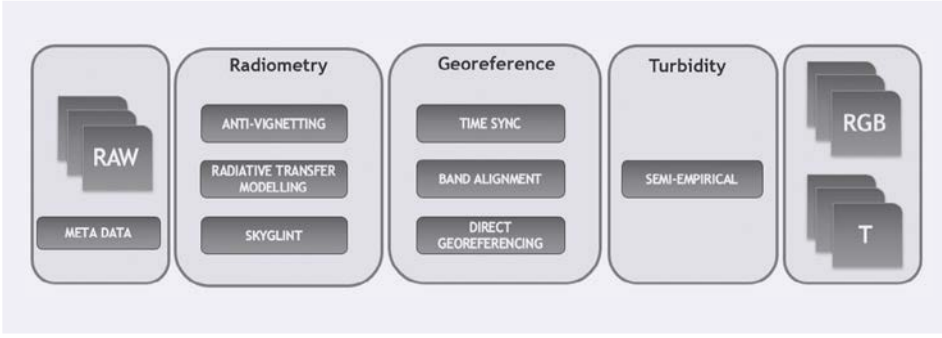

FIGURE 6

Schematic overview of the drone image processing chain to convert raw data into meaningful biophysical units and truecolour products.

leaving reflectance. The latter quantity is of interest because the light travelled through the water column and thus bears information regarding (optical) characteristics like turbidity. The first step performs an anti-vignetting of the image. Vignetting is the darkening of the image towards the edges and can be corrected for by normalising with a calibrated reference image. Secondly, the radiance signal received by the sensor can be converted into physically meaningful water-leaving reflectance through radiative transfer modelling. The at-sensor radiance (Lat-sens) is the sum of the atmospheric radiance (Latm), the specular reflection at the water surface (Lspec) and the water-leaving radiance (Lw):

$$L_{at-sens} = L_{atm} + L_{spec} + L_w$$

(1)

The specular reflection consists of two components: direct reflection of sun light, also called sun glint (Lr,sun), and scattering of the atmosphere to the water surface and reflected into the detector, i.e. sky glint (Lr,sky):

$$L_{spec} = L_{r,sun} + L_{r,sky}$$

(2)

When processing drone images, two assumptions can be made:

1. drones fly at limited height (especially when compared to satellites), so Latm can be neglected, and
2. the camera of the drone is slightly tilted to avoid sun glint and thus the LLrr,ssssss component can be ignored. This is however a simplification of reality, since the pixels of a frame camera have different viewing angles and (waves at the water surface can lead to occurrence of sun glint within the image.

The simplified radiative transfer formula is:

$$L_{at-sens} = L_{r,sky} + L_w$$

(3)

The sky glint contribution is modelled with the iCOR image processing tool (De Keukelaere et al., 2018) adapted for drone imagery. iCOR is an image-based atmospheric correction tool which relies on Moderate-Resolution Atmospheric Radiance and Transmittance Model – version 5 (MODTRAN5) (Berk et al., 2006) Look-Up-Tables (LUTs) to solve the radiative transfer equation based on a set of input parameters. The input parameters are height, solar and viewing angles and simulated cloud type and coverage (open sky, cumulus, stratus, etc.).

The quality of interest is water leaving reflectance (ρw), which is an optical property of water and can be related to bio-physical parameters like turbidity. ρw is expressed as:

$$\rho_w = \frac{L_w}{E_d} \pi$$

(4)

with Ed as the downwelling irradiance. The value for downwelling irradiance can be obtained from either spectral reference targets present in the field or an irradiance sensor mounted on the drone. An irradiance sensor allows to capture changing light conditions continuously, but is very sensitive to its viewing angle and is not straightforward to process. One of the difficulties in this perspective is the separation of direct sun light on the sensor and diffuse light. This separation is not measured in situ but must be done in post-processing. Its strong dependence on cloud cover, sensor orientation and time of the day make it more a backup solution. Nevertheless, advances are expected in the years to come. Another solution to measure irradiance is the use of spectral reference panels. They have a known and calibrated reflectance value (albedo) over the complete panel and can be fixed on a boat or at the shore-side. These panels have been used in the Texel case, and are depicted in Figure 7. The drone has to fly over these panels, and only the light conditions at the moment of the overpass are captured. When the measured radiance from the camera can be coupled with the known reflectance value, other measured radiance values

The radiometric step converts the raw drone imagery from digital numbers to water leaving reflectance.

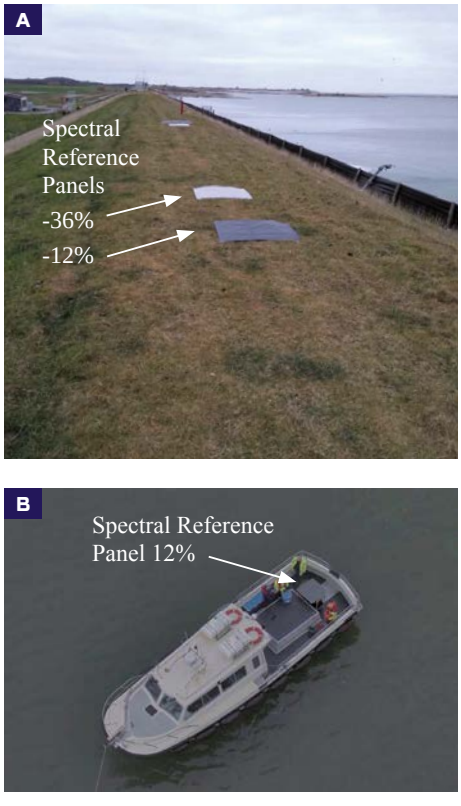

FIGURE 7

Two types of spectral reference panels placed at the shore-side (A) and fixed on a boat (B), with known spectral behavior. The light target has an albedo of 36%, while the albedo of the darker target is 12%.

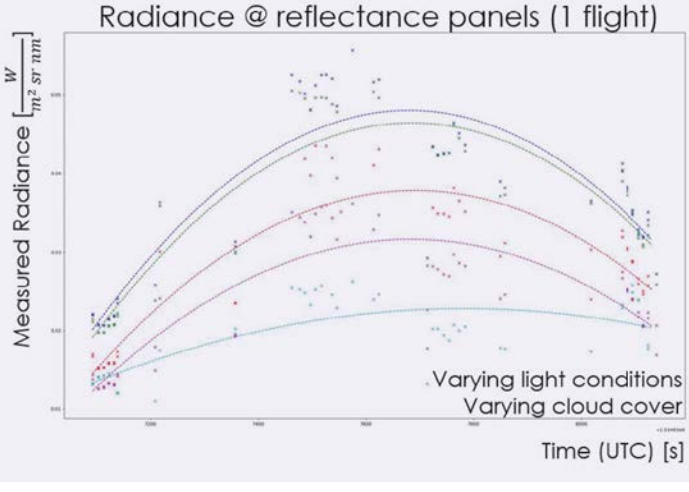

FIGURE 8

Radiance measured by the spectral reference panels (dots) for the 5 spectral bands of the MicaSense RedEdge camera. The lines show the interpolated results through the flight.

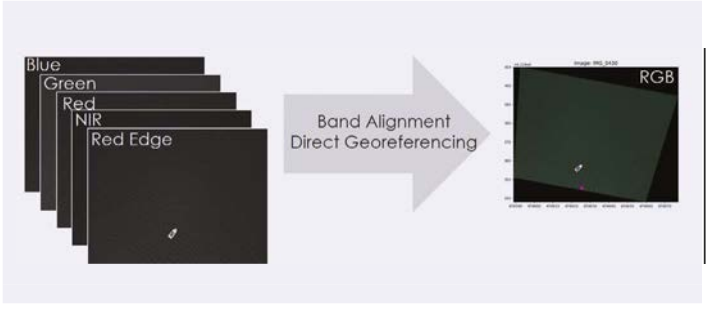

FIGURE 9

Schematic overview of the geometric correction.

can be translated into reflectance through interpolation. This method has satisfying results for uniform cloud conditions (like most of the Texel case) but is less appropriate under strong variations in cloud cover (patchy). Figure 8 shows the evolution of the measured radiance for the five spectral bands at the reflectance panels through one flight (approximately 15 minutes). From this figure, it becomes clear that using only the reflectance values at the start and end of the flight is not sufficient to cover the variations in light conditions.

Geometric correction

To know which part of the water body the drone image is covering, the images are georeferenced. A time synchronised triggering between the camera and auxiliary sensors is of utmost importance, since in a fraction of a second, the drone can be shifted or rotated and looks at a different part of the water surface. The separate spectral bands of the camera are aligned before the images are projected based on position, altitude and orientation of the drone and camera recorded by the GPS/IMU. In contrast to land application, no fixed recognisable features are present in water bodies, which excludes the use of structure-for motion techniques (Westoby *et al.*, 2012). The precision of the drone's auxiliary sensors determines the geometric accuracy of the final product which is projected through the so-called direct geo-referencing technique. A GPS system provides information on latitude, longitude and height of the camera, while an IMU sensor captures the roll, pitch and yaw of the camera. Applying translation, rotation, projection on a flat surface (water) and image warping results in an image georeferenced in space. Figure 9 summarises the geometric correction step.

Turbidity retrieval

Turbidity derived from optical drone data are expressed in Formazin Nephelometric Units (FNU) units, according to the definition of the International Standards Organisation ISO 7027 (ISO, 1999), using the 90° side-scattering of light at 860 nm with respect to Formazin, a chemical standard. Although these units are slightly different compared to the continuous turbidity meter with units in NTU (see Section 2.3), both can be intercompared.

Turbidity (T) was derived using the formula of Dogliotti et al. (2015), without calibration or fine-tuning of the algorithm based on in-situ measurements:

$$T = \frac{A^{\lambda}\,\rho_w(\lambda)}{(1-\rho_w(\lambda)/C^{\lambda})}\ [\mathrm{FNU}] \quad (5)$$

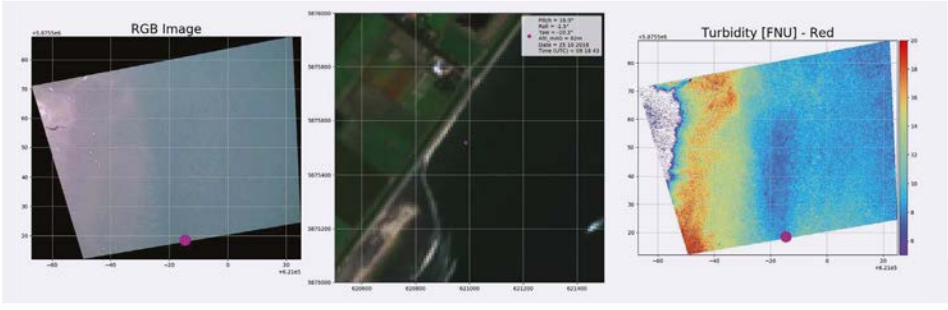

FIGURE 10

Drone image acquired at 09:18:43 UTC (53.016° N, 4.804° E). On the left the truecolour image and on the right the derived turbidity product is shown. The photo in the middle shows the position of the drone with a purple spot. This purple spot is also added in the truecolour and the turbidity maps.

FIGURE 11

Drone image acquired at 09:45:32 UTC (53.014° N, 4.804° E). On the left the truecolour image and on the right the derived turbidity product is shown. The photo in the middle shows the position of the drone with a purple spot.

FIGURE 12

Drone image acquired at 11:49:24 UTC (53.016° N, 4.804° E). On the left the truecolour image and on the right the derived turbidity product is shown. The photo in the middle shows the position of the drone with a purple spot.

With A and C two wavelength-dependent (λ) calibration coefficients. Aλ and Cλ have been calculated for the MicaSense RedEdge camera through spectral resampling, which yielded a value of 366.14 and 0.19563 respectively. When an extensive match-up database is available for a specific region, these calibration coefficients can be further fine-tuned. As the amount of match-ups in Texel was limited in space and time, the collected in-situ data was only used for validation.

Results

Figures 10-12 show a few individual drone images captured during the test with corresponding derived turbidity product. The picture in the middle shows the location of the drone with a purple dot. This dot is also added in the truecolour and the turbidity map. The images were acquired on respectively 09:18:43, 09:45:32 and 11:49:24 UTC time.

Figure 13 shows the mosaic created from different individual images captured during one flight. A first limited validation is shown in Figure 14. These first results show that realistic values can be obtained from drone imagery.

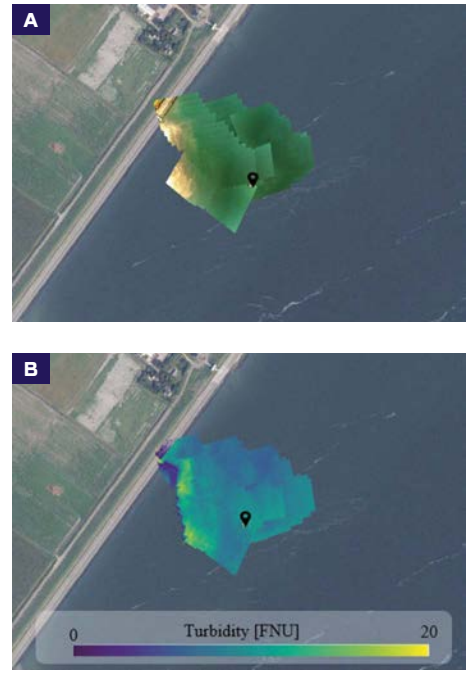

FIGURE 13

Mosaic of Truecolour images (A) and turbidity (B) captured during one flight. The location of the boat is highlighted with a black marker.

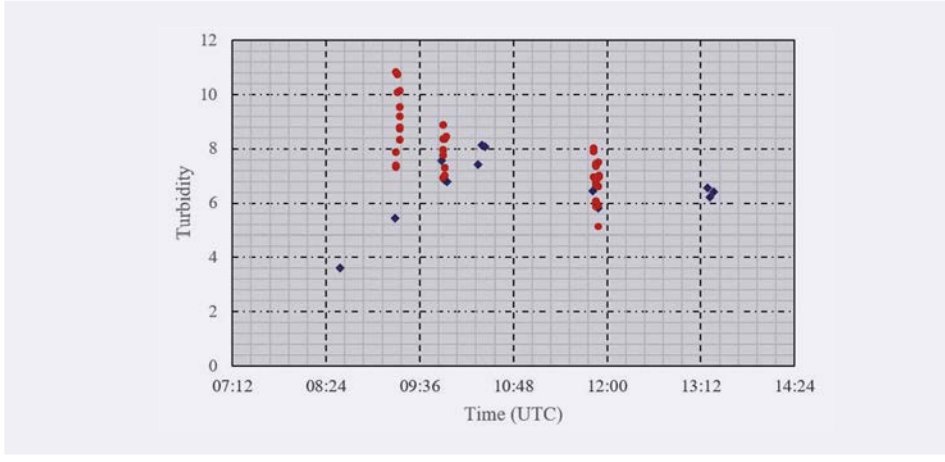

FIGURE 14

Validation of the turbidity measurements, expressed in FNU (red dots) with the reference in-situ data, in NTU (blue dots). Each red dot originates from a single image. Since images where captured every few seconds, multiple drone results are obtained during one in-situ data collection.

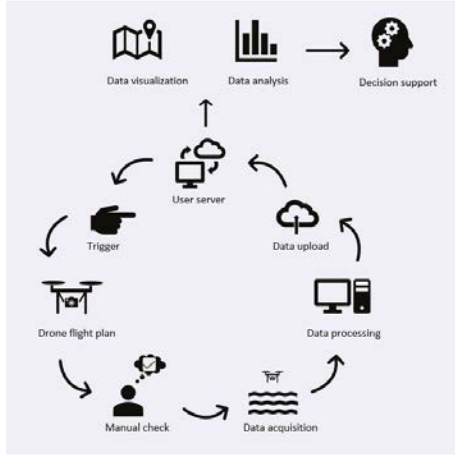

FIGURE 15

Conceptual representation of the (semi-) autonomous drone data collection.

During the drone flight, images were captured every few seconds. From each of these images the derived turbidity concentrations were extracted, which explains the different red dots (i.e. drone observations) around one in-situ measurement in Figure 14. The observed scattering can be caused by wave effects, changes in light conditions or viewing angles. By including noise filtering techniques this scattering can be reduced.

The turbidity values observed in the test area are very low, which means that small difference in absolute values can lead to large errors. Despite the small validation dataset available, turbidity values obtained from drone imagery are within the range of in-situ measurements. The offset around 09:30 can be related to inaccurate modelling of the cloud conditions. Through novel validation campaigns in waters covering a wider range of turbidity values, a larger validation database can be established, leading to a better understanding of the limitations and characterising the accuracy and uncertainty of this technology.

Outlook

Through field campaigns, the drone image processing chain can be further improved and validated. We will also investigate in solutions for improving signal-to-noise ratios and deriving time series information out of these datasets. To facilitate the collection of airborne drone data, a set of operational protocols will be generated that explain users how to collect such data over water bodies, taking into account the different challenges that have to be tackled.

The next step is to launch an end-to-end image processing solution, MAPEO, for water applications (https://remotesensing.vito.be/case/mapeo). Currently, MAPEO is available for drone-based phenotyping. Stakeholders can order drone flights, perform drone flights or order a pilot. They can upload their drone collected data on the online platform which are quality checked and performs image processing and analytics through cloud computing.

Going even one step further, we are evaluating a semi-autonomous drone data collection architecture where a drone can be triggered by other sensors (e.g. continuous turbidity buoy that detects an increased signal) and performs a predefined flight mission. The collected data can be automatically uploaded, processed and visualised (or downloaded) by the user in their preferred spatial data infrastructure. This will allow easy interpretation and data analysis. The concept of this process is schematically depicted in Figure 15.

Although drone data only capture information of the top-layer of the water column, it provides insight on the propagation of the sediment plume at the water surface. This information can be inserted in sediment modelling tools, together with in-situ turbidity measurements at different depths. At the end, a complete picture of the sediment plume propagation in three dimensions might become feasible.

Conclusion

In contrast to earlier presented work (Raymaekers et al., 2017), this study shows the performance of airborne drone data under sub-optimal illumination conditions for optical sensors: i.e. varying cloud conditions. The test site was the dune construction site in Texel, where dredging activities were performed by Jan De Nul Group. Through an automated image processing tool, raw airborne drone data were converted into physically meaningful water leaving reflectance values and further into projected turbidity maps. This without any calibration or fine-tuning of the implemented algorithms. Simultaneous with the drone flight, reference in-situ data were collected for validation of the dataset. A first limited validation, based on data captured during one day at one location, yielded realistic values. The drone flights in this project were executed with a custom made drone hardware, but efforts are being made to work with drone systems that are easily accessible for other users.

Summary

At the end of October 2018, a pilot test case at the Prins Hendrik Zanddijk project in Texel, The Netherlands, was organised to demonstrate drone technology for water quality monitoring. Jan De Nul was working on creating a new dune area seaward of the existing dike. This dune takes over the coastal protection function of the existing dyke and combines it with nature development, public services and recreational appeal. For the demo an octocopter drone platform, Altura Zenith ATX8, was used with a multispectral camera, MicaSense RedEdge M, underneath.

During drone flights, a base station shows real-time information on the location of the drone, a projected truecolour image captured by the camera and the position of neighbouring boats through Automatic Identification System (AIS). Thanks to this information it is easy to adapt flight missions according to the situation. The drone data were processed with dedicated software into turbidity maps. This independently from in-situ observations. Water samples, collected simultaneously with drone flights were used for the validation of the derived products.

First presented as a paper at the CEDA Dredging Days Conference 2019 in Rotterdam, this article has been published in a slightly adapted version with permission of the copyright holder, CEDA. At the conclusion of the conference, IADC's Secretary General René Kolman bestowed the Young Author Award to Liesbeth De Keukelaere to recognise her outstanding paper and presentation of the paper 'Mapping water quality with drones – test case in Texel'.

This project received funding from the European Union's Horizon 2020 research and innovation programme under grant agreement No 776480.

REFERENCES

Berk A., Anderson G.P., Acharya P.K., Bernstein L.S. & Muratov L. (2006)
MODTRAN5: 2006 update. *Proceedings of SPIE 6233, Algorithms and Technologies for Multispectral, Hyperspectral, and Ultraspectral Imagery* XII, 62331F.

De Keukelaere L., Sterckx S., Adriaensen S., Knaeps E., Reusen I., Giardino C., Bresciani M., Hunter P., Neil C., Van der Zande D & Vaiciute D. (2018)
Atmospheric correction of Landsat-8/OLI and Sentinel-2/MSIdata using iCOR algorithm: validation for coastal and inland waters. *European Journal of Remote Sensing*, Vol. 51, No. 1, 525-542.

Dogliotti A., Ruddick K., Nechad B., Doxaran D. & Knaeps, E. (2015)
A single algorithm to retrieve turbidity from remotely-sensed data in all coastal and estuarine waters. *Remote Sensing of Environment*, Vol. 156, 157-168.

Environmental Protection Agency (EPA) of the United States. (1993)
Method 180.1: Determination of Turbidity by Nephelometry. EPA, 180.1-10.

Han Y.G., Jung S.H. & Kwon O. (2017)
How to utilize vegetation survey using drone image and image analysis software. *Journal of Ecology and Environment*, Vol. 41, No.18.

International Organisation for Standardization (ISO). (1999)
Water quality – Determination of turbidity. ISO, p. 7027.

Ishida T., Kurihara J., Viray F.A., Namuco S.B., Paringit E., Perez G.J., Takahashi Y. & Marciano J.J. (2018)
A novel approach for vegetation classification using UAV-based hyperspectral imaging. *Computers and Electronics in Agriculture*. Vol. 144, 80-85.

Kay S., Hedley J. & Lavender S. (2009)
Sun glint correction of high and low spatial resolution images of aquatic scenes: a review of methods for visible and near-infrared wavelengths. *Remote sensing,* Vol. 1, 697-730.

Raymaekers D., De Keukelaere L., Knaeps E., Strackx G., Decrop B. & Bollen M. (2017)
Integrated approach to monitor water dynamics with drones. *CEDA Dredging Days 2017 – Sustainable Dredging – Continued Benefits.*

Westoby M.J., Brasington J., Glasser N.F., Hambrey M. J. & Reynolds J. M. (2012)
'Structure-from-Motion' photogrammetry: A low-cost, effective tool for geoscience applications. *Geomorphology*, Vol. 179, 300–314.

At the conclusion of the CEDA Dredging Days Conference 2019, IADC's Secretary General René Kolman bestowed the Young Author Award to Liesbeth De Keukelaere to recognise her outstanding paper and presentation of the paper 'Mapping water quality with drones – test case in Texel'.

Els Knaeps
Els holds a Master's degree in Geography and an advanced Master's degree in GIS and Remote Sensing. She started working at VITO as a junior scientist focusing on satellite and airborne image processing for water quality retrieval. She is now team leader water and coastal applications at VITO Remote Sensing.

Robrecht Moelans
Robrecht is working with VITO as R&D Professional in processing drone and satellite images for water and coastal applications. Before VITO, Robrecht worked as R&D Project Manager with G-tec in Liège, Belgium and as Operational Superintendent (expat) with dredging company Jan De Nul. He holds Master's degree in Mining and Geotechnical Engineering from Katholieke Universiteit Leuven.

Liesbeth De Keukelaere
Liesbeth is a R&D Professional at VITO with a Master's degree in Bio-Science Engineering. During her first year after graduation, Liesbeth worked on spectral unmixing techniques to distinguish different tree species within one pixel. She then shifted her attention to water applications, investigating remote sensing's potential for water quality monitoring in inland, coastal and transitional waters.

Gert Strackx
Gert is a System Integration Engineer at VITO Remote Sensing working on multispectral cameras and other types of sensors on UAS platforms in combination with high-end INS for lightweight environments using 3D design and additive manufacturing techniques. He holds a Master's degree in Electronics and Telecommunications.

Emile Lemey
Emile works as Project Development Engineer at Jan de Nul Group. His background is in Bioengineering and Marine conservation. At Jan De Nul he has focused on nature based solutions projects in which ecological considerations are an essential part of the design phase. He worked as Environmental Engineer on the Prins Hendrik Zanddijk project during the realisation phase.